Autodisplay of an endo-1,4-β-xylanase from *Clostridium cellulovorans* in *Escherichia coli* for xylans degradation

Victor E. Balderas Hernández[1], Carlos J. Salas-Montantes[1], Ana P. Barba-De la Rosa, and Antonio De Leon-Rodriguez*.

División de Biología Molecular. Instituto Potosino de Investigación Científica y Tecnológica (IPICYT), Camino a la Presa de San José 2055 Lomas 4ª. Sección C.P. 78216, San Luis Potosí, S.L.P., México.

[1]These authors contributed equally.

*Corresponding author

E-mail: aleonr@me.com, aleonr@ipicyt.edu.mx

Victor E, Balderas Hernández ORCID: 0000-0002-3295-6758

Ana Paulina Barba-De la Rosa ORCID: 0000-0003-4999-036X

Antonio De León-Rodríguez ORCID: 0000-0003-3347-3499

Running title: Autodisplay of a xylanase in *E. coli.*

Submitted to: Enzyme Microbial Technology

Abstract

The goal of this work was the *autodisplay* of the endo β-1,4-xylanase (XynA) from *Clostridium cellulovorans* in *Escherichia coli* using the AIDA system to carry out whole-cell biocatalysis and hydrolysate xylans. For this, pAIDA-xynA vector containing a synthetic *xynA* gene was fused to the signal peptide of the toxin subunit B *Vibro cholere* (ctxB) and the auto-transporter of the synthetic *aida* gene, which encodes for the connector peptide and β-barrel of the auto-transporter (AT-AIDA). *E. coli* TOP10 cells were transformed and the biocatalyst was characterized using beechwood xylans as substrate. Optimal operational conditions were temperature of 55°C and pH 6.5, and the Michaelis-Menten catalytic constants V_{max} and K_m were 4.14 x 10^{-2} mg/mL/min (149 U/g_{DCW}) and 6.01 mg/mL, respectively. Xylanase activity was inhibited by Cu^{2+}, Zn^{2+} and Hg^{2+} as well as EDTA, detergents, and organic acids, and improved by Ca^{2+}, Co^{2+} and Mn^{2+} ions. Ca^{2+} ion strongly enhanced the xylanolytic activity up to 2.4-times when 5 mM $CaCl_2$ were added. Also, Ca^{2+} improved enzyme stability at 60 and 70°C. Results suggest that pAIDA-xynA vector has the ability to express functional xylanase to perform whole-cell biocatalysis in order to hydrolysate xylans from hemicellulose feedstock.

Keywords: AIDA; autodisplay; hemicellulose; whole cell biocatalysts; xylanase.

1. Introduction.

Hemicellulose is the second most abundant polysaccharide on earth after cellulose, and they together structure the vegetal biomass. The hemicellulose contains β-(1→4) linked pentoses units, being xylans (composed by xylose and arabinose) the main components of the polymer [1]. Thus xylans are an attractive raw material to produce prebiotics (that will

48 stimulate the growth of benefic microorganism in the gastrointestinal tract), packaging
49 coatings, to release fermentable carbohydrates to produce biofuels, or other value-added
50 metabolites [2–4]. To obtain units of xylose, xylans must be hydrolyzed through thermal,
51 chemical or enzymatic methods. In this sense, endo-1,4-β-xylanases (EC 3.2.1.8) catalyze
52 the hydrolysis of β-1,4-xylans into xylo-oligosaccharides of variable length and D-xylose
53 [5,6]. Enzymatic hydrolysis of xylans is the most efficient method to release the monomers
54 without the production of toxic compounds such as formic acid or furfural [7,8], however
55 the use of enzymes is an expensive method. Therefore, extensive approaches have been
56 implemented to obtain functional and re-utilizable biocatalysts [9,10]. Re-utilizable
57 biocatalysts can be obtained through enzymatic immobilization, *i.e.* the whole-cell catalysis
58 approach. This will allow the *autodisplay* of enzymes in the outer membrane of microbial
59 cells [11–13]. Enzyme autodisplay has the advantages that the enzymes are continuously
60 regenerated, no purification after production is required, the enzyme is stabilized,
61 prolonging its half-life time, the surface area of reaction is higher in comparison with other
62 immobilization techniques, the catalysis occurs in the extracellular medium, and therefore it
63 has a reduction of the resistance of the mass transfer of the substrate to the enzyme [14–16].
64 The Auto-Transporter *Adhesin Involved in Diffuse Adherence* (AT-AIDA), is a protein
65 autodisplay system from *E. coli* that has been used to efficiently display proteins, epitopes
66 and enzymes in *E. coli*'s surface [17–20]. AIDA autotransporter can export more than
67 100,000 recombinant protein units per single cell, a characteristic that has been used for the
68 development of different biotechnological applications, specially those focused to generate
69 biocatalysis on the cell surface [11].
70 In this work, an endo-1,4-β-xylanase (XynA) from *Clostridium cellulovorans* was
71 expressed into *Escherichia coli* using an optimized synthetic gene, *xynA*, that was fused to

the autotransporter *aida* gene. The whole cell biocatalyst was tested using synthetic and natural substrates to obtain its kinetic and enzymatic characteristics.

2. Materials and methods

2.1 Design and construction of artificial XynA-AIDA system

A synthetic *xynA* gene was designed using the protein sequence of the endo-1,4-β-xylanase (XynA) from *Clostridium cellulovorans* (GenBank: AAN32825.1). The *xynA* sequence was redesigned to optimize the codon usage for its correct expression in *E. coli.* The expression plasmid contained: (1) The constitutive *gapAP1* promoter drives the *aida-xynA* gene expression, (2) the signal peptide of the toxin subunit β *Vibro cholere* (ctxB, UniProtKB - E3UUX3) to translocate the polypeptide into the internal membrane, and (3) the *aida* auto-transporter gene which encodes for the connector peptide and β-barrel (aminoacids from 839 to 1,286, GenBank X65022.1), fused with the optimized *xynA* gene. DNA sequence was modified using GenScript Co. (New Jersy, USA) to eliminate internal restriction sites and to codon-optimize it prior its synthesis. The resulting sequence was designated as *aida-xynA* gene, which was flanked by the *Nde*I and *Bam*HI restriction sites. The *aida-xynA* gene has a longitude of 3,176 pb, which encodes for a fusion protein of 965 amino acid residues. The resulting DNA construction was synthetized by Biomatik Corp. (Delaware, USA) and cloned into the pUC57 vector (Thermo Fisher Scientific) using the *Eco*RV sites. The resulting plasmid was named as pAIDA-xynA (Fig. 1). Codon Adaptation Index was calculated for the native and optimized sequences [21].

2.2. Bacterial strain and growth conditions

E. coli TOP-10 strain was transformed with the pAIDA-xynA plasmid by electroporation. Cells were routinely grown at 37°C in Luria-Bertani (LB) medium, containing 250 μg/mL of ampicillin (Sigma-Aldrich). Solid media were prepared by the addition of agar (1.5% w/v).

2.3. Endo-1,4-β-xylanases activity visualization

To visualize the endo-1,4-β-xylanase activity, cells of *E. coli* TOP10/pAIDA-xynA were cultured in 24 well-plates with LB solid medium plus 0.2% of the chromogenic compound RBB-Xylan (4-o-methyl-D-glucurono-D-xylan Ramazol Brilliant Blue, RBB, Sigma-Aldrich) and 150 μg/mL of ampicillin. Then, 0.5 μL of cell suspension with an optical density at 600 nm (OD_{600}) of 10 were spot-cultivated and incubated at 37°C for 24 h, where 1 OD_{600} was equivalent to 0.37 g (dry cell weigh, DCW)/L. Non-transformed *E. coli* TOP10 cells were also cultured under same conditions as negative control.

2.4. Enzymatic reaction in the whole cells

The enzymatic assay was performed using the method reported for glycolytic immobilized enzymes [22,23] as follows: 10 mL of LB medium with 250 μg/mL ampicillin were inoculated with cells of *E. coli* TOP10/pAIDA-xynA at 37°C and shaking at 200 rpm until an OD_{600} of 1 was attained. Then cells were collected by centrifugation at 16,089 x*g* and washed twice with the reaction buffer (0.1 M acetate buffer pH 6.5). Enzymatic reactions were carried with 1 mL of cells at an OD_{600} of 10 and using 1% of soluble beechwood xylans (Sigma-Aldrich) as substrate. Temperature, pH and $CaCl_2$ concentration of the

reaction was modified according sections 2.5, 2.6 and 2.6, respectively. For the optimal conditions, the enzymatic reaction was incubated at 55°C, pH 6.5, at 1,400 rpm for 30 min. The reactions were stopped by centrifugation at 16,089 x*g* for 5 min and 250 µL the supernatant (diluted, if required) was used to measure the enzymatic activity by the 3,5-Dinitro Salicylic Method (DNS), as described below. This protocol was also used for the following sections for the evaluation of the effects of temperature, pH, Ca^{2+}, and metal ions.

2.5. Effect of temperature and pH on the biocatalyst activity

The effect of temperature on the biocatalyst activity was assessed by incubation of 1 mL of cells at an OD_{600} of 10 in the reaction buffer containing 1% beechwood xylans as described above, at temperatures ranging from 30 to 70°C, at 1,400 rpm for 30 min. For the effect of pH, the assays were done at different pH (4-8) using the universal Britton and Robinson´s buffer (50 mM phosphoric acid, 50 mM boric acid and 50 mM acetic acid), supplemented with 1% beechwood xylans, and incubated at 55°C and 1,400 rpm for 30 min. Negative controls of reaction using medium cell free were also included. All the experiments were performed in triplicate.

2.6. Thermal stability of the biocatalyst

To estimate the thermal stability, 1 mL of cells at an OD_{600} of 10 were incubated in the reaction buffer (0.1 M acetate buffer pH 6.5) at 55, 60, 70 and 80°C for 15, 30, 45 and 60

138 min, with or without addition of $CaCl_2$ 5mM. After the corresponding incubation, cells
139 were transferred into ice for 5 min. Residual activity was measured by incubating cells at
140 55°C for 30 min at 1,400 rpm, with 1% beechwood xylans. The negative controls (cell-free)
141 were also evaluated. The activity of cells assayed at 55°C was defined as 100%.
142

143 *2.7. Effect of calcium on biocatalyst*

144 The effect of Ca^{2+} ion on the biocatalyst was determined by incubation in Britton and
145 Robinson´s buffer pH 6.5 at 55°C at 1,400 rpm for 30 min with 1% beechwood xylans and
146 with calcium chloride ranging from 0 to 10 mM. The negative controls (cell-free) were also
147 evaluated. The activity assayed in the absence of calcium was defined as 100%.
148

149 *2.8. Effect of metal ions, detergents and organic inhibitors*

150 The effect of 1 mM of metals: $ZnCl_2$, NaCl, KCl, $CoCl_2$, $CuCl_2$, $FeCl_3$, $MgCl_2$, $MnCl_2$,
151 $NiCl_2$, $HgCl_2$, and $Pb(C_2H_3O_2)_2$, detergents: EDTA, SDS, Tween 80, DTT and TRITON
152 X100, and organic inhibitors present in lignocellulosic hydrolysates: acetic acid (20 mM),
153 formic acid (10 mM) and furfural (0.5 mM) was determined by incubation of 1 mL of cells
154 at an OD_{600} of 10 in reaction buffer (0.1 M acetate buffer pH 6.5). For each treatment, cells
155 were incubated at 55°C for 30 min, at 1,400 rpm, with 1% beechwood xylans. The negative
156 controls (cell-free) were also evaluated. The activity assayed in the absence of metals,
157 detergents or organic inhibitors was defined as 100%.
158

159 *2.9. Kinetic parameters calculation*

160 The Michaelis-Menten constants were estimated using the enzyme activity assay with cell
161 suspension at OD_{600} of 5 and different initial substrate concentrations from 0 to 20 mg/mL
162 beechwood xylans in Britton and Robinson´s buffer (pH 6.5) at 55°C by 2 h under constant
163 agitation at 1,400 rpm. Kinetic constants (V_{max} and K_m) were calculated using the Hanes-
164 Woolf equation [24] using standard linear regression technique.

165

166 *2.10. Determination of enzyme activity*

167 The endo-1,4-β-xylanase activity was determined by measuring the reducing sugars
168 released during xylans hydrolysis by 3,5-Dinitro Salicylic Method (DNS) [25] with some
169 modifications. The reaction mixture contained 250 µL of supernatant from centrifuged
170 samples (diluted in water, if required) and 750 µL of DNS reagent, the reaction mixture
171 was boiled for 5 min at 100°C and stopped by cooling to room temperature. The
172 absorbance was measured at 595 nm in microplate reader (BioRad). Xylose, (Sigma) in the
173 range of 0.15 to 6 mg/mL, was used as the calibration curve for total reducing sugar
174 determination. 1 U was defined as the amount of enzyme that releases 1 µmol of reducing
175 sugars per minute, and for the biocatalyst specific activity as one activity unit of biocatalyst
176 per mg of *E. coli* cells.

177

178 *2.11. Statistical analysis*

179 The statistical analysis of the experiments was determined by analysis of variance

(ANOVA) and unpaired Student´s t-test. Treatments with $p < 0.05$ were considered as statistically significant. The statistical analysis was performed using Microsoft Excel v16.0 and GraphPad Prism v5.

3. Results and discussion

3.1 *Design of aida-XynA cassette*

The pAIDA-XynA plasmid of 5,922 pb was constructed to confer the ability on *E. coli* to hydrolysate xylans through the expression of the synthetic gene fusion *aida-xynA* (Fig. 1). The open reading frame (ORF) was codon optimized for its expression in *E. coli*. The original *aida-xynA* gene had a Codon Adaptation Index of 0.59 and after the optimization it was 0.95, which is an indicator of the improvement in its efficiency of translation [21]. The percentage of GC was reduced from 63.44 to 54.05%, and all the internal restriction sites and the sequences similar to Shine-Delgarno (SD) into the ORF were discarded. Strategic restriction sites (*Asc*I and *Xho*I) were also included to allow the substitution of the *xynA* gene by other genes of interest, and *Eco*R1-*Bam*HI sites for subcloning the entire cassette including the gapA promoter, into other plasmids. The molecular elements of the cassette are: The *gapAP1* promoter, optimal SD sequence for *E. coli*, *ctxB* signal peptide from *Vibrio cholera,* synthetic *xynA* gene encoding for the endo-β-1,4- xylanase from *C. cellulovorans,* and the synthetic *aida* gene encoding β-barrel (AT-AIDA) from *E. coli* (Fig. 1). AIDA autotransporter has been successfully used to display different enzymes for whole cell biocatalysis. For instance, tyrosinase Tyr1 from *Bacillus megaterium* was functionally expressed in the surface of *E. coli* in order to oxidize externally added tyrosine to produce

melanin biopolymer [26]. Enzyme methyl parathion hydrolase was expressed on the surface of *E: coli* by fusing it with the AIDA autotransporter, in order to degrade methyl parathion [27]. Gustavsson et al. [28] fused *aida* gene with the gene for an *Arthrobacter citreus* ω-transaminase variant (AcωTA) to allow *E. coli* to produce chiral amines in the supernatant culture. A carboxylesterase, EstA from *Burkholderia gladioli* fused to AIDA anchor molecule, was displayed on the surface of *E. coli* to gain the esterase activity over p-nitrophenylacetate [29]. Also, a metabolically engineered *E. coli* was transformed with the fusion AIDA-AmyA to express α-amylase from *Bacillus megaterium* to hydrolyze starch, and to simultaneously produce ethanol and hydrogen [22].

3.2 Detection of endo-β-xylanolytic activity on plate

To visualize the xylanolytic activity as a result of the transformation with the pAIDA-XynA into *E. coli*, a qualitative plate assay was done. The enzyme activity was observed by the change of the intense blue color to a smoother tone on blue (Fig. 2). This change was better visualized in a gray scale images. As noted in Fig. 2A and B, cells harboring the plasmid pAIDA-XynA presented a halo around the bacterial colony, whereas the colony of control cells, the halo was not observed (Fig 2C and D). Colorimetric assay corroborated the functionality of the pAIDA-xynA since the xylanolytic activity gained by the *E. coli* cells, is the result of the transcriptional, translational events as well as the translocation of the polypeptide (SP-xylanase-β-barrel) to the periplasm space by the Sec secretion system, excision of the signal peptide, and posterior *autodisplay* by the auto-transporter through the outer membrane. The RBB assay has been used successfully to detect the xylanolitic activity in *E. coli* cells expressing a xylanase of *Thermomyces lanuginosus* fused to Lpp-

OmpA protein [30] and in the autodisplay of a xylanase from *Trichoderma reesei* in the surface of *Saccharomyces cerevisiae* [31].

3.3 Effect of pH and temperature and thermal stability of the biocatalyst

The effect of pH on the activity of the biocatalyst was evaluated in the range 4 to 8. As showed in Fig. 3a, the maximum activity was attained at pH 6.5, and it decreased at pH 8 showing a 30% of the relativity activity. The optimum pH value for the biocatalyst (6.5) is similar to those reports for xylanases from mesophilic bacteria, such as the free endo-1,4-β-xylanase from *Bacillus licheniformis* [32], and an immobilized xylanase from *Bacillus subtilis* fused to the protein expansin [33]. The effect of temperature was assessed in the range of 30 to 70°C using 1% of soluble xylans. As noted in the Fig. 3b, the enzyme activity increased from 5.6 to 100% when temperature increased from 30 to 55°C, after that, the relative enzyme activity decreased to 7.3% at 70°C. Therefore, the optimum temperature for the biocatalyst was 55°C. Kosugi et al. reported 60°C and pH 5 as the optimal conditions for the free endo-1,4-β-xylanase from *C. cellulovorans* [34]. These differences with respect to the enzyme immobilized reported here, could be explained as result of the anchorage of the enzyme into the cell-wall of *E. coli*, which induced changes in the thermodynamic properties of the xylanase by the union to the AIDA auto-transporter [35]. These changes in the optimal conditions could be an advantage for its application at large scale, because a lower temperature reduces the use of energy, and a pH closest the neutral is easier to reach [36,37].

The thermal stability of the xylanase was evaluated at temperatures above the optimal observed (Fig. 4). The xylanase remained active after a treatment of 60 min at 60°C, decreasing only at 83% with respect of the control (cells incubated at 55°C). The activity of

the enzyme at 70°C decreased at 43% in the first 15 min of incubation, maintaining only 15% after 60 min of incubation. When cells were incubated at 80°C for 15 min, xylanase activity fell at 28%, and reached only 7% at 30 min of incubation, remaining this low at the following incubation times (Fig. 4). A similar thermal stability profile was described for the Xyn10B xylanase of *Caldicellulosiruptor lactoaceticus*, in which activity was conserved at 65°C, but it was lost after 30 min of incubation at 70°C [38]. Optimum temperature-activity (Table 1) and thermal stability for the *E. coli*-immobilized XynA from *C. cellulovorans* are in the range of temperatures of previously reported GH11 xylanases [39,40].

3.4 Effect of calcium and thermal stability

The effect of Ca^{2+} ion on the biocatalyst was performed under optimal conditions of temperature and pH (55°C and 6.5, respectively). As shown in Fig. 5, the enzyme activity increased 2.4-times when 5 mM of $CaCl_2$ where added to the reaction mix, the same effect was observed with 10 mM $CaCl_2$. This positive effect of Ca^{2+} to increase the enzyme activity of the endo-1,4-β-xylanase from *C. cellulovorans* was also reported by Yazawa et al. [41] for the xylanase from alkaliphilic *Bacillus* sp. strain 41M-1 (Table 1). On the contrary, 10 mM of Ca^{2+} inhibited the activity of endo-1,4-β-xylanase from *Cellulomonas fimi* [42], and caused a slight decrease in the activity of Xyn10B from *Acidothermus cellulolyticus* [43]. Whereas, 10 mM of Ca^{2+} improved the activity of xynB from *Xanthomonas axonopodis* pv. *citri* towards beechwood xylan. Calcium ions are structurally necessary for the maintenance of the geometry of XynB active site, Ca^{2+} absence caused a negative effect on the substrate recognition and binding [44].

Besides improving the enzymatic activity, Ca^{2+} ions improved the thermal stability of XynA. As observed in fig. 4, cells treated with $CaCl_2$, showed an improved residual activity

after incubation at 60 and 70°C. Specially at 70°C, cells without calcium addition its activity dropped at 70 and 43% at 15 and 30 min of incubation, respectively. In contrast, when 5 mM of $CaCl_2$ was added, XynA activity remained at 90 and 70%, respectively, indicating its thermal protective effect (Fig. 4). Even when Ca^{2+}-treated cells were incubated for 15 min at 80°C, the residual activity was 1.5-times higher in comparison with cells without calcium addition. A similar effect was observed for XYLA from *Pseudomonas fluorescens* subsp. *cellulosa*. Although enzyme activity was not significantly improved under optimal conditions, 1mM of Ca^{2+} protected XYLA from thermal inactivation and proteolytic (chymotrypsin) attack, in comparison with reactions using 1mM EDTA or enzyme versions without Ca^{2+} binding sites [44]. The addition of 5 mM of Ca^{2+} improved the thermostability of the Xyn10A from thermophilic bacteria *Thermotoga thermarum*, and its activity was 400% improved when 1 mM of Ca^{2+} was present [45].

The endo-1,4-β-xylanase from *C. cellulovorans* is composed by three distinct functional domains (Figure 6). The glycosyl hydrolase domain from family 11 (GH11), that runs from amino acid 32 to 227 [46,47]; The carboxy-terminal domain corresponds to the NodB deacetylase, located from amino acid 319 to 497, that removes acetyl groups from acetylated xylan [48] and the central domain of XynA corresponds to the Dockerin I, spanning amino acids 224 to 311. This domain plays a function as cohesin and participates in the formation of the bacterial cellulosome [49]. The dockerin I contains a conserved feature residue pattern (D [NDT] x x D [DEN] x x D), this dockerin repeats can bind two Ca^{2+} ions, as observed in Fig. 6, this residue repeats are highly conserved among xylanolytic microorganisms. The positive effect of Ca^{2+}, described for the XynA of *C. cellulovorans*, has been reported for xylanases of *Clostridium* strain BOH3 [50]. *C thermocellum* [51,52], *Clostridium saccharoperbutylacetonicum*, and other GH11

298 xylanases [53]. Also, Ca^{2+} induces the correct folding of the dockerin into its tertiary
299 structure essential for the cohesin binding, required for the union with the substrate in *C.*
300 *thermocellum* [54]. As observed for other carbohydrate hydrolases, for example the
301 cellohydrolase from *C. thermocellum* where Ca^{2+} plays a central role on its stability and
302 contributes to its thermo stability [55]. These results indicate, that the addition of calcium
303 ions will ensure that calcium-binding sites are occupied improving the endo-1,4-β-xylanase
304 activity and its stability.
305
306 *3.5 Effect of metal, detergents and organic inhibitors*
307 The effect of metals on the activity of *E. coli*-immobilized XynA was also evaluated. As
308 observed in figure 7, 1 mM of Na^{+}, Mg^{2+}, or Pb^{2+} ions caused a mild inhibition (0-15%) of
309 XynA activity. Meanwhile Cu^{2+} and Zn^{2+} ions caused a 25 and 43% decrease, respectively,
310 Hg^{2+} caused a higher inhibitory effect, cells pre-treated with 1mM showed only an 8.2% of
311 the activity observed in the untreated cells (control, Fig. 7). Similar inhibitory effects by
312 Hg^{2+}, Cu^{2+} and Zn^{2+} have been described for xylanases from *Aspergillus ficuum* [56],
313 *Penicillum glabrum* [57], *P. sclerotiorum* [58], and *Bacillus* sp. strain K-1 [59]. Strong
314 inhibitory effect of Hg^{2+} has been explained by its ability to interact with sulfhydryl groups
315 of cysteine residues, inducing conformational changes that might alter the catalytic or
316 stabilizing domains of xylanases [60,61].
317 Interestingly, 1 mM of Mn^{2+} or Co^{2+}, improved the xylanase activity by 1.15- and 1.4-times
318 (Fig. 7), respectively. Likely, 2 mM of Co^{2+} or Mn^{2+} ions caused an increment in the
319 relative activity of the recombinant xylanase from *Streptomyces coelicolor* Ac-738 [62].
320 Relative enzyme activity was increased by 20 and 85% when purified xylanase from
321 *Bacillus subtilis* ASH was incubated with 1 mM of $CoCl_2$ and $MnCl_2$, respectively [63].

Further analysis are required to determine if Co^{2+} and Mn^{2+} ions participate in the formation of hydrophobic, ionic or disulfide interactions that might result in an improved stabilization of the *E. coli*-immobilized XynA structure.

Detergents and chelators effects on XynA activity were also evaluated. 1 mM of EDTA, SDS, tween-80, or Triton-x100 caused a minor decrease, ranged between 9-16%, in the residual activity of the xylanase enzyme (Fig. 7). EDTA could act as a chelator, trapping metals that are required for proper enzyme folding, such as Ca^{2+}, as previously described [44]. SDS will interfere with the formation of hydrophobic interactions required for maintaining the structure of the xylanase, as previously described [57,64].

A final set of compounds was evaluated for its effects on XynA activity, fomic acid, acetic acid and furfural. As observed in figure 7, activity of XynA was reduced by 36% when *E. coli* cells were pre-treated with 10 mM of formic acid. 20 mM of acetic acid and 0.5 mM of furfural caused a minor inactivation of the enzyme (Fig. 7). These three compounds and its evaluated concentrations were selected based on its presence and abundance in lignocellulosic hydrolysates [65,66] that might interfere with the activity of the xylanase. As observed for *E. coli*-immobilized XynA, from a group of 11 inhibitors, 0.5 g/L (10.8 mM) of formic acid caused the higher decrease in the xylans hydrolysis rate of 44.49 %, followed by acetic acid and furfural, but in a lower extent. The mechanism of action of formic acid on the xylanase, according with its kinetic parameter analysis, it's a mixed-inhibition (competitive and uncompetitive) mechanism [67].

3.6 Michaelis-Menten parameters

The initial velocity of the endo-1,4-β-xylanase followed a typical Michael-Menten kinetics as the xylans concentration was increased in the range of 0 to 20 mg/mL (Fig. 8). V_{max} and

346 K_m were determined using to regression of the Hanes-Woolf plot and the values were 4.14
347 x10^{-2} mg/mL/min (149 U/g_{DCW}) and 6.01 mg/mL. Table 1 summarizes the K_m values and
348 the specific enzyme activities for some free and immobilized endo-1,4-β-xylanases. The K_m
349 for the immobilized endo-1,4-β-xylanase by the AIDA system reported here (6.01 mg/mL)
350 was similar to those values of K_m reported for the free xylanase from *Clostridium*
351 *acetobutyllicum* (6 mg/mL, larchwood xylans) [68]. Since the immobilization of the
352 enzyme, it would be valuable to further perform an analysis using the heterogeneous
353 catalysis approach's kinetics. Immobilized xylanases, in alginate, Q-sepharose or agar-agar
354 showed variable values of *Km* constants, ranged between 5.38 -10.97 mg/mL (Table 1).
355 The *E. coli*-AIDA-immobilized XynA meets the described range [69–71]. Kumar et al [72]
356 showed that alginate bed-immobilization of xylanase from *B. licheniformis* strain Alk-1
357 improved the 4ºC-30 days storage stability (80%) in comparison with the free enzyme
358 (5%), besides improving their recycling efficiency up to five reaction cycles. Xylanase
359 immobilization has shown to have a positive effect in retaining their activity after several
360 recycling cycles, also improving their temperature and pH tolerance, in contrast with their
361 free-enzyme version Table 1 [69,70,73].
362 Immobilization of xylanases on the surface of microorganisms has not been extensively
363 reported, and thus there is no available information of the kinetic constants. Xylanases have
364 been expressed on the surfaces of yeast; XYNII from *T. reesei* fused to the yeast-agglutinin
365 in *S. cerevisiae* [31], a xylanase from a rumen fosmid library fused to the surface
366 membrane protein Aga1 in *S. cerevisiae* [74], xylanase xyn from *Paenibacillus polymyxa*
367 PPL-3 using Aga2p as an anchor protein in *S. cerevisiae* [75], xylanase TxXYN from
368 *Thermobacillus xylanilyticus* fused to cell wall proteins YlPir, YlCWP1 and YlCBM in
369 *Yarrowia lipolytica* [76]. Also, have been displayed in *E. coli*: the XynA xylanase from T.

lanuginosus was fused to Lpp-OmpA protein for its expression on the surface of *E. coli*, able to degrade oat-spelt-xylans, at optimal pH of 6.2 and 65ºC [30], similar to those obtained for *E. coli*-AIDA-immobilized XynA. Xylanase XyloA from *Fusarium graminearum* was fused with anchor protein Blc, in order to degrade beechwood xylans by *E. coli* [77]. Endo-1,4-β-xylanase from *Aspergillus fumigatus* was fused to the ice nucleation protein (INP) anchor from *Erwinia ananas* IN-10 InaA for its display in *E. coli* BL21-SI surface [78]. In the best of our knowledge this is the first report of the utilization of the AIDA system for the autodisplay of a functional xylanase in the surface of *E. coli*.

4. Conclusions

The synthetic construction encoding the fusion protein constituted by the ctxB signal peptide, endo-1,4-β-xylanase, β-barrel AT-AIDA was transcriptional, translational and post-translational processed efficiently by *E. coli.* The whole-cell biocatalyst through the AIDA auto-transporter and using beechwood xylans as substrate, shows an optimal xylanolytic activity at 55°C and pH 6.5. Cu^{2+}, Zn^{2+} and Hg^{2+} as well as EDTA, detergents, and organic acids are inhibitors, whereas Co^{+2}, Mn^{+2} and Ca^{2+} increase the enzymatic activity. Also, the Ca^{2+} ion improves thermal stability of the xylanase. The enzyme follows a Michaelis-Menten kinetics behavior with a K_m of 6.01 mg/mL. The expression of glycolytic enzymes such as the endo-1,4-β-xylanases on the surface of *E. coli* cells is an effective method for enzyme immobilization to hydrolysate complex substrates such as the xylans.

Funding

This work was partially supported by CONACyT Ciencias Básicas Grant 281700.

Declaration of Competing Interest

None

Acknowledgments

CJ Salas-Montantes thanks to the National Council of Science and Technology (CONACyT) for his scholarship No: 590382.

References

[1] H.V. Scheller, P. Ulvskov, Hemicelluloses, Annu. Rev. Plant Biol. 61 (2010) 263–289. https://doi.org/10.1146/annurev-arplant-042809-112315.

[2] L. Sun, Y.-S. Jin, Xylose Assimilation for the Efficient Production of Biofuels and Chemicals by Engineered *Saccharomyces cerevisiae,* Biotechnol. J. n/a (2020) 2000142. https://doi.org/10.1002/biot.202000142.

[3] H. Zhu, W. Luo, P.N. Ciesielski, Z. Fang, J.Y. Zhu, G. Henriksson, M.E. Himmel, L. Hu, Wood-Derived Materials for Green Electronics, Biological Devices, and Energy Applications, Chem. Rev. 116 (2016) 9305–9374. https://doi.org/10.1021/acs.chemrev.6b00225.

[4] H.P. Vu, L.N. Nguyen, M.T. Vu, M.A.H. Johir, R. McLaughlan, L.D. Nghiem, A comprehensive review on the framework to valorise lignocellulosic biomass as biorefinery feedstocks, Sci. Total Environ. 743 (2020) 140630. https://doi.org/https://doi.org/10.1016/j.scitotenv.2020.140630.

[5] D. Dodd, I.K.O. Cann, Enzymatic deconstruction of xylan for biofuel production, GCB Bioenergy. 1 (2009) 2–17. https://doi.org/10.1111/j.1757-1707.2009.01004.x.

[6] R. Biswas, A. Persad, V.S. Bisaria, Production of Cellulolytic Enzymes, in: Bioprocess. Renew. Resour. to Commod. Bioprod., John Wiley & Sons, Inc., Hoboken, NJ, USA, 2014: pp. 105–132. https://doi.org/10.1002/9781118845394.ch5.

[7] K. Kucharska, P. Rybarczyk, I. Hołowacz, R. Łukajtis, M. Glinka, M. Kamiński, Pretreatment of Lignocellulosic Materials as Substrates for Fermentation Processes, Molecules. 23 (2018) 2937. https://doi.org/10.3390/molecules23112937.

[8] O.B. Chukwuma, M. Rafatullah, H.A. Tajarudin, N. Ismail, Lignocellulolytic Enzymes in Biotechnological and Industrial Processes: A Review, Sustainability. 12 (2020) 7282. https://doi.org/10.3390/su12187282.

[9] S. Santos, J. Puna, J. Gomes, A Review on Bio-Based Catalysts (Immobilized Enzymes) Used for Biodiesel Production, Energies. 13 (2020) 3013. https://doi.org/10.3390/en13113013.

[10] Y. Osbon, M. Kumar, Biocatalysis and Strategies for Enzyme Improvement, in: Biophys. Chem. - Adv. Appl., IntechOpen, 2020. https://doi.org/10.5772/intechopen.85018.

[11] J. Jose, T.F. Meyer, The Autodisplay Story, from Discovery to Biotechnical and Biomedical Applications, Microbiol. Mol. Biol. Rev. 71 (2007) 600–619. https://doi.org/10.1128/mmbr.00011-07.

[12] P. Van Ulsen, K.M. Zinner, W.S.P. Jong, J. Luirink, On display: Autotransporter secretion and application, FEMS Microbiol. Lett. 365 (2018). https://doi.org/10.1093/femsle/fny165.

[13] E. van Bloois, R.T. Winter, H. Kolmar, M.W. Fraaije, Decorating microbes: Surface display of proteins on *Escherichia coli*, Trends Biotechnol. 29 (2011) 79–86.

https://doi.org/10.1016/j.tibtech.2010.11.003.

[14] K.S. Lam, Application of Whole-Cell Biotransformation in the Pharmaceutical Industry, in: Biocatal. Pharm. Ind., John Wiley & Sons, Ltd, Chichester, UK, 2009: pp. 213–227. https://doi.org/10.1002/9780470823163.ch10.

[15] C.C.C.R. de Carvalho, Enzymatic and whole cell catalysis: Finding new strategies for old processes, Biotechnol. Adv. 29 (2011) 75–83. https://doi.org/https://doi.org/10.1016/j.biotechadv.2010.09.001.

[16] B. Lin, Y. Tao, Whole-cell biocatalysts by design, Microb. Cell Fact. 16 (2017) 106. https://doi.org/10.1186/s12934-017-0724-7.

[17] C. Detzel, R. Maas, J. Jose, Autodisplay of Nitrilase from Alcaligenes faecalis in E. coli Yields a Whole Cell Biocatalyst for the Synthesis of Enantiomerically Pure (R)-Mandelic Acid, ChemCatChem. 3 (2011) 719–725. https://doi.org/10.1002/cctc.201000382.

[18] N.T. Nhan, E.G. de Valdivia, M. Gustavsson, T.N. Hai, G. Larsson, Surface display of *Salmonella* epitopes in *Escherichia coli* and *Staphylococcus carnosus*, Microb. Cell Fact. 10 (2011) 22. https://doi.org/10.1186/1475-2859-10-22.

[19] E. Kranen, C. Detzel, T. Weber, J. Jose, Autodisplay for the co-expression of lipase and foldase on the surface of *E. coli*: Washing with designer bugs, Microb. Cell Fact. 13 (2014) 19. https://doi.org/10.1186/1475-2859-13-19.

[20] S. Sichwart, I.E.P. Tozakidis, M. Teese, J. Jose, Maximized Autotransporter-Mediated Expression (MATE) for surface display and secretion of recombinant proteins in *Escherichia coli*, Food Technol. Biotechnol. 53 (2015) 251–260. https://doi.org/10.17113/ftb.53.03.15.3802.

[21] P. Sen, A. Waris, S.K. Ray, S.S. Satapathy, A Web Portal to Calculate Codon

Adaptation Index (CAI) with Organism Specific Reference Set of High Expression Genes for Diverse Bacteria Species, in: Springer, Singapore, 2020: pp. 319–325. https://doi.org/10.1007/978-981-15-0633-8_31.

[22] A.K. Gutiérrez-García, C.L. Alvarez-Guzmán, A. De Leon-Rodriguez, Autodisplay of alpha amylase from *Bacillus megaterium* in *E. coli* for the bioconversion of starch into hydrogen, ethanol and succinic acid, Enzyme Microb. Technol. 134 (2020) 109477. https://doi.org/https://doi.org/10.1016/j.enzmictec.2019.109477.

[23] T. Maehara, H. Yagi, T. Sato, M. Ohnishi-Kameyama, Z. Fujimoto, K. Kamino, Y. Kitamura, F.S. John, K. Yaoi, S. Kaneko, GH30 glucuronoxylan-specific xylanase from *Streptomyces turgidiscabies* C56, Appl. Environ. Microbiol. 84 (2018). https://doi.org/10.1128/AEM.01850-17.

[24] C.S. Hanes, Studies on plant amylases, Biochem. J. 26 (1932) 1406–1421. https://doi.org/10.1042/bj0261406.

[25] A. Jain, R. Jain, S. Jain, Quantitative Analysis of Reducing Sugars by 3, 5-Dinitrosalicylic Acid (DNSA Method), in: Humana, New York, NY, 2020: pp. 181–183. https://doi.org/10.1007/978-1-4939-9861-6_43.

[26] M. Gustavsson, D. Hörnström, S. Lundh, J. Belotserkovsky, G. Larsson, Biocatalysis on the surface of *Escherichia coli*: Melanin pigmentation of the cell exterior, Sci. Rep. 6 (2016) 1–9. https://doi.org/10.1038/srep36117.

[27] J. Yang, R. Liu, H. Jiang, Y. Yang, C. Qiao, Selection of a whole-cell biocatalyst for methyl parathion biodegradation, Appl. Microbiol. Biotechnol. 95 (2012) 1625–1632. https://doi.org/10.1007/s00253-011-3792-3.

[28] M. Gustavsson, M.N. Muraleedharan, G. Larsson, Surface expression of ω-transaminase in *Escherichia coli*, Appl. Environ. Microbiol. 80 (2014) 2293–2298.

https://doi.org/10.1128/AEM.03678-13.

[29] E. Schultheiss, C. Paar, H. Schwab, J. Jose, Functional esterase surface display by the autotransporter pathway in *Escherichia coli*, J. Mol. Catal. B Enzym. 18 (2002) 89–97. https://doi.org/10.1016/S1381-1177(02)00063-2.

[30] W. Qu, Y. Xue, Q. Ding, Display of Fungi Xylanase on *Escherichia coli* Cell Surface and Use of the Enzyme in Xylan Biodegradation, Curr. Microbiol. 70 (2015) 779–785. https://doi.org/10.1007/s00284-015-0781-2.

[31] Y. Fujita, S. Katahira, M. Ueda, A. Tanaka, H. Okada, Y. Morikawa, H. Fukuda, A. Kondo, Construction of whole-cell biocatalyst for xylan degradation through cell-surface xylanase display in *Saccharomyces cerevisiae*, J. Mol. Catal. B Enzym. 17 (2002) 189–195. https://doi.org/https://doi.org/10.1016/S1381-1177(02)00027-9.

[32] A. Ghosh, S. Sutradhar, D. Baishya, Delineating thermophilic xylanase from *Bacillus licheniformis* DM5 towards its potential application in xylooligosaccharides production, World J. Microbiol. Biotechnol. 35 (2019) 1–18. https://doi.org/10.1007/s11274-019-2605-1.

[33] B. Wu, Q. Yu, S. Chang, M.M. Pedroso, Z. Gao, B. He, G. Schenk, Expansin assisted bio-affinity immobilization of endoxylanase from *Bacillus subtilis* onto corncob residue: Characterization and efficient production of xylooligosaccharides, Food Chem. 282 (2019) 101–108. https://doi.org/10.1016/j.foodchem.2019.01.004.

[34] A. Kosugi, K. Murashima, R.H. Doi, Xylanase and acetyl xylan esterase activities of XynA, a key subunit of the *Clostridium cellulovorans* cellulosome for xylan degradation, Appl. Environ. Microbiol. 68 (2002) 6399–6402. https://doi.org/10.1128/AEM.68.12.6399-6402.2002.

[35] I. Gawarzewski, F. DiMaio, E. Winterer, B. Tschapek, S.H.J. Smits, J. Jose, L.

Schmitt, Crystal structure of the transport unit of the autotransporter adhesin involved in diffuse adherence from *Escherichia coli*, J. Struct. Biol. 187 (2014) 20–29. https://doi.org/https://doi.org/10.1016/j.jsb.2014.05.003.

[36] E.C. Agbo, Innovations in Biotechnology, InTech, 2012. https://doi.org/10.5772/2450.

[37] V.M. Cardoso, G. Campani, M.P. Santos, G.G. Silva, M.C. Pires, V.M. Gonçalves, R. de C. Giordano, C.R. Sargo, A.C.L. Horta, T.C. Zangirolami, Cost analysis based on bioreactor cultivation conditions: Production of a soluble recombinant protein using *Escherichia coli* BL21(DE3), Biotechnol. Reports. 26 (2020) e00441. https://doi.org/10.1016/j.btre.2020.e00441.

[38] X. Jia, Y. Han, The extracellular endo-β-1,4-xylanase with multidomain from the extreme thermophile *Caldicellulosiruptor lactoaceticus* is specific for insoluble xylan degradation, Biotechnol. Biofuels. 12 (2019) 143. https://doi.org/10.1186/s13068-019-1480-1.

[39] V. Kumar, J. Marín-Navarro, P. Shukla, Thermostable microbial xylanases for pulp and paper industries: trends, applications and further perspectives, World J. Microbiol. Biotechnol. 32 (2016) 1–10. https://doi.org/10.1007/s11274-015-2005-0.

[40] G. Paës, J.G. Berrin, J. Beaugrand, GH11 xylanases: Structure/function/properties relationships and applications, Biotechnol. Adv. 30 (2012) 564–592. https://doi.org/10.1016/j.biotechadv.2011.10.003.

[41] R. Yazawa, J. Takakura, T. Sakata, Ihsanawati, R. Yatsunami, T. Fukui, T. Kumasaka, N. Tanaka, S. Nakamura, A calcium-dependent xylan-binding domain of alkaline xylanase from alkaliphilic *Bacillus* sp. strain 41M-1, Biosci. Biotechnol. Biochem. 75 (2011) 379–381. https://doi.org/10.1271/bbb.100730.

[42] S. Khanna, Gauri, Regulation, purification, and properties of xylanase from *Cellulomonas fimi*, Enzyme Microb. Technol. 15 (1993) 990–995. https://doi.org/https://doi.org/10.1016/0141-0229(93)90177-4.

[43] S. Shahid, R. Tajwar, M.W. Akhtar, A novel trifunctional, family GH10 enzyme from *Acidothermus cellulolyticus* 11B, exhibiting endo-xylanase, arabinofuranosidase and acetyl xylan esterase activities, Extremophiles. 22 (2018) 109–119. https://doi.org/10.1007/s00792-017-0981-8.

[44] C.R. Santos, Z.B. Hoffmam, V.P. De Matos Martins, L.M. Zanphorlin, L.H. De Paula Assis, R.V. Honorato, P.S.L. De Oliveira, R. Ruller, M.T. Murakami, Molecular mechanisms associated with xylan degradation by xanthomonas plant pathogens, J. Biol. Chem. 289 (2014) 32186–32200. https://doi.org/10.1074/jbc.M114.605105.

[45] H. Shi, Y. Zhang, X. Li, Y. Huang, L. Wang, Y. Wang, H. Ding, F. Wang, A novel highly thermostable xylanase stimulated by Ca2+ from *Thermotoga thermarum*: Cloning, expression and characterization, Biotechnol. Biofuels. 6 (2013) 26. https://doi.org/10.1186/1754-6834-6-26.

[46] D.G. Naumoff, Hierarchical classification of glycoside hydrolases, Biochem. 76 (2011) 622–635. https://doi.org/10.1134/S0006297911060022.

[47] J. Wicki, J. Schloegl, C.A. Tarling, S.G. Withers, Recruitment of both uniform and differential binding energy in enzymatic catalysis: Xylanases from families 10 and 11, Biochemistry. 46 (2007) 6996–7005. https://doi.org/10.1021/bi700359e.

[48] J.I. Laurie, J.H. Clarke, A. Ciruela, C.B. Faulds, G. Williamson, H.J. Gilbert, J.E. Rixon, J. Millward-Sadler, G.P. Hazlewood, The NodB domain of a multidomain xylanase from *Cellulomonas fimi* deacetylates acetylxylan, FEMS Microbiol. Lett.

148 (1997) 261–264. https://doi.org/10.1016/S0378-1097(97)00046-3.

[49] A.L. Carvalho, F.M.V. Dias, J.A.M. Prates, T. Nagy, H.J. Gilbert, G.J. Davies, L.M.A. Ferreira, M.J. Romão, C.M.G.A. Fontes, Cellulosome assembly revealed by the crystal structure of the cohesin-dockerin complex, Proc. Natl. Acad. Sci. U. S. A. 100 (2003) 13809–13814. https://doi.org/10.1073/pnas.1936124100.

[50] G. Rajagopalan, J. He, K.L. Yang, Direct fermentation of xylan by *clostridium* strain BOH3 for the production of butanol and hydrogen using optimized culture medium, Bioresour. Technol. 154 (2014) 38–43. https://doi.org/10.1016/j.biortech.2013.11.094.

[51] S. Chauvaux, H. Souchon, P.M. Alzari, P. Chariot, P. Beguin, Structural and functional analysis of the metal-binding sites of *Clostridium thermocellum* endoglucanase CelD, J. Biol. Chem. 270 (1995) 9757–9762. https://doi.org/10.1074/jbc.270.17.9757.

[52] S.K. Choi, L.G. Ljungdahl, Structural role of calcium for the organization of the cellulosome of *Clostridium thermocellum*, Biochemistry. 35 (1996) 4906–4910. https://doi.org/10.1021/bi9524631.

[53] W. Qu, W. Shao, Cloning, expression and characterization of glycoside hydrolase family 11 endoxylanase from *Bacillus pumilus* ARA, Biotechnol. Lett. 33 (2011) 1407–1416. https://doi.org/10.1007/s10529-011-0568-x.

[54] B.L. Lytle, B.F. Volkman, W.M. Westler, J.H.D. Wu, Secondary structure and calcium-induced folding of the *Clostridium thermocellum* dockerin domain determined by NMR spectroscopy, Arch. Biochem. Biophys. 379 (2000) 237–244. https://doi.org/10.1006/abbi.2000.1882.

[55] I.A. Kataeva, V.N. Uversky, L.G. Ljungdahl, Calcium and domain interactions

585 contribute to the thermostability of domains of the multimodular cellobiohydrolase,
586 CbhA, a subunit of the *Clostridium thermocellum* cellulosome, Biochem. J. 372
587 (2003) 151–161. https://doi.org/10.1042/BJ20021621.
588 [56] F. Lu, M. Lu, Z. Lu, X. Bie, H. Zhao, Y. Wang, Purification and characterization of
589 xylanase from *Aspergillus ficuum* AF-98, Bioresour. Technol. 99 (2008) 5938–5941.
590 https://doi.org/10.1016/j.biortech.2007.10.051.
591 [57] A. Knob, S.M. Beitel, D. Fortkamp, C.R.F. Terrasan, A.F. De Almeida, Production,
592 purification, and characterization of a major *Penicillium glabrum* xylanase using
593 brewer's spent grain as substrate, Biomed Res. Int. 2013 (2013).
594 https://doi.org/10.1155/2013/728735.
595 [58] A. Knob, E.C. Carmona, Purification and characterization of two extracellular
596 xylanases from *Penicillium sclerotiorum*: A novel acidophilic xylanase, Appl.
597 Biochem. Biotechnol. 162 (2010) 429–443. https://doi.org/10.1007/s12010-009-
598 8731-8.
599 [59] K. Ratanakhanokchai, K.L. Kyu, M. Tanticharoen, Purification and properties of a
600 xylan-binding endoxylanase from Alkaliphilic *Bacillus* sp. strain K-1., Appl.
601 Environ. Microbiol. 65 (1999) 694–7. https://doi.org/10.1128/AEM.65.2.694-
602 697.1999.
603 [60] Q.K. Beg, M. Kapoor, L. Mahajan, G.S. Hoondal, Microbial xylanases and their
604 industrial applications: A review, Appl. Microbiol. Biotechnol. 56 (2001) 326–338.
605 https://doi.org/10.1007/s002530100704.
606 [61] G. Gupta, V. Sahai, R.K. Gupta, Thermal stability and thermodynamics of xylanase
607 from *Melanocarpus albomyces* in presence of polyols and salts, BioResources. 9
608 (2014) 5801–5816. https://doi.org/10.15376/biores.9.4.5801-5816.

[62] A. V. Lisov, O. V. Belova, Z.I. Andreeva-Kovalevskaya, Z.I. Budarina, A.A. Solonin, N.G. Vinokurova, A.A. Leontievsky, Recombinant xylanase from *Streptomyces coelicolor* Ac-738: Characterization and the effect on xylan-containing products, World J. Microbiol. Biotechnol. 30 (2014) 801–808. https://doi.org/10.1007/s11274-013-1480-4.

[63] A. Sanghi, N. Garg, V.K. Gupta, A. Mittal, R.C. Kuhad, One-step purification and characterization of cellulase-free xylanase produced by alkalophilic *Bacillus subtilis* ASH, Brazilian J. Microbiol. 41 (2010) 467–476. https://doi.org/10.1590/S1517-83822010000200029.

[64] L.A. de O. da Silva, C.R.F. Terrasan, E.C. Carmona, Purification and characterization of xylanases from *Trichoderma inhamatum*, Electron. J. Biotechnol. 18 (2015) 307–313. https://doi.org/10.1016/j.ejbt.2015.06.001.

[65] S. Larsson, E. Palmqvist, B. Hahn-Hägerdal, C. Tengborg, K. Stenberg, G. Zacchi, N.O. Nilvebrant, The generation of fermentation inhibitors during dilute acid hydrolysis of softwood, Enzyme Microb. Technol. 24 (1999) 151–159. https://doi.org/10.1016/S0141-0229(98)00101-X.

[66] S.M. Davies, R.S. Linforth, S.J. Wilkinson, K.A. Smart, D.J. Cook, Rapid analysis of formic acid, acetic acid, and furfural in pretreated wheat straw hydrolysates and ethanol in a bioethanol fermentation using atmospheric pressure chemical ionisation mass spectrometry, Biotechnol. Biofuels. 4 (2011) 28. https://doi.org/10.1186/1754-6834-4-28.

[67] I. Maulana Hidayatullah, T. Setiadi, M. Tri Ari Penia Kresnowati, R. Boopathy, Xylanase inhibition by the derivatives of lignocellulosic material, Bioresour. Technol. 300 (2020) 122740. https://doi.org/10.1016/j.biortech.2020.122740.

[68] S.F. Lee, C.W. Forsberg, J.B. Rattray, Purification and characterization of two endoxylanases from *Clostridium acetobutylicum* ATCC 824, Appl. Environ. Microbiol. 53 (1987) 644–650. https://doi.org/10.1128/aem.53.4.644-650.1987.

[69] M. Kapoor, R.C. Kuhad, Immobilization of xylanase from *Bacillus pumilus* strain MK001 and its application in production of xylo-oligosaccharides, Appl. Biochem. Biotechnol. 142 (2007) 125–138. https://doi.org/10.1007/s12010-007-0013-8.

[70] Z. Bibi, F. Shahid, S.A. Ul Qader, A. Aman, Agar-agar entrapment increases the stability of endo-β-1,4-xylanase for repeated biodegradation of xylan, Int. J. Biol. Macromol. 75 (2015) 121–127. https://doi.org/10.1016/j.ijbiomac.2014.12.051.

[71] M. Irfan, J. Kiran, S. Ayubi, A. Ullah, Q.U.A. Rana, S. Khan, F. Hasan, M. Badshah, A.A. Shah, Immobilization of β-1,4-xylanase isolated from *Bacillus licheniformis* **S3**, J. Basic Microbiol. 60 (2020) 600–612. https://doi.org/10.1002/jobm.202000077.

[72] S. Kumar, I. Haq, J. Prakash, A. Raj, Improved enzyme properties upon glutaraldehyde cross-linking of alginate entrapped xylanase from *Bacillus licheniformis*, Int. J. Biol. Macromol. 98 (2017) 24–33. https://doi.org/10.1016/j.ijbiomac.2017.01.104.

[73] P. Kumar, A. Gupta, S.R. Dhakate, R.B. Mathur, S. Nagar, V.K. Gupta, Covalent immobilization of xylanase produced from *Bacillus pumilus* SV-85S on electrospun polymethyl methacrylate nanofiber membrane, Biotechnol. Appl. Biochem. 60 (2013) 162–169. https://doi.org/10.1002/bab.1072.

[74] J.K. Wang, B. He, W. Du, Y. Luo, Z. Yu, J.X. Liu, Yeast with surface displayed xylanase as a new dual purpose delivery vehicle of xylanase and yeast, Anim. Feed Sci. Technol. 208 (2015) 44–52. https://doi.org/10.1016/j.anifeedsci.2015.07.002.

[75] S. Yeasmin, C.H. Kim, H.J. Park, M.I. Sheikh, J.Y. Lee, J.W. Kim, K.K. Back, S.H.

Kim, Cell surface display of cellulase activity-free xylanase enzyme on *Saccharomyces cerevisiae* EBY100, Appl. Biochem. Biotechnol. 164 (2011) 294–304. https://doi.org/10.1007/s12010-010-9135-5.

[76] S. Duquesne, S. Bozonnet, F. Bordes, C. Dumon, J.-M. Nicaud, A. Marty, Construction of a Highly Active Xylanase Displaying Oleaginous Yeast: Comparison of Anchoring Systems, PLoS One. 9 (2014) e95128. https://doi.org/10.1371/journal.pone.0095128.

[77] M. Zhao, Z. Zheng, T. Chen, Expressing xylanases in *Escherichia coli* by cell surface display, in: Adv. Mater. Res., Trans Tech Publications Ltd, 2013: pp. 965–969. https://doi.org/10.4028/www.scientific.net/AMR.634-638.965.

[78] M.Y.J. Wee, A.M. Abdul, F.D. Abu Bakar, K.O. Low, R. Md Illias, Expression of xylanase on *Escherichia coli* using a truncated ice nucleation protein of Erwinia ananas (InaA), Process Biochem. 78 (2019) 25–32. https://doi.org/10.1016/j.procbio.2019.01.005.

[79] Z. Han, F. Shang-Guan, J. Yang, Molecular and biochemical characterization of a bimodular xylanase from marinifilaceae bacterium strain SPP2, Front. Microbiol. 10 (2019). https://doi.org/10.3389/fmicb.2019.01507.

[80] W.B. Vieira, L.R.D.S. Moreira, A.M. Neto, E.X. Ferreira Filho, Production and characterization of an enzyme complex from a new strain of *Clostridium thermocellum* with emphasis on its xylanase activity, Brazilian J. Microbiol. 38 (2007) 237–242. https://doi.org/10.1590/S1517-83822007000200009.

[81] A. Kosugi, K. Murashima, R.H. Doi, Characterization of xylanolytic enzymes in *Clostridium cellulovorans*: Expression of xylanase activity dependent on growth substrates, J. Bacteriol. 183 (2001) 7037–7043.

https://doi.org/10.1128/JB.183.24.7037-7043.2001.

684 **Table1.** Comparison of specific enzyme activity of the endo-1,4-β-xylanase *E. coli*-AIDA-

685 immobilized XynA and K_m values for some biocatalysts reported in the literature.

Microorganism	Optimum Temperature (C)	Optimum pH (-)	Catalyst conditions	Ca^{2+} effect	K_m	Reference
Bacillus licheniformis S3	60	3.0–11.0	Ca^{2+} alginate-immobilized	-	10.97 mg/mL	[71]
B. pumilus strain MK001	63	6.5	Ionic binding with Q-sepharose	-	8.2 mg/mL with Birchwood xylan	[69]
B. pumilus strain MK001	60	6.0	Free enzyme	-	7.9 mg/mL with Birchwood xylan	[69]
Geobacillus stearothermophilus	60	7.0	Immobilized in agar-agar	-	0.507 mg/min with xylan	[70]
Geobacillus stearothermophilus	50	7.0	Free enzyme	-	0.523 mg/min with xylan	[70]
B. licheniformis strain Alk-1	60	9.0	Glutaraldehyde activated Ca^{2+} alginate beads	-	5.38 mg/mL with beechwood xylan	[72]
B. licheniformis strain Alk-1	50	8.0	Free enzyme	-	4.36 mg/mL with beechwood xylan	[72]
Cellulomonas fimi	45	5.0	Purified by gel filtration	Inhibited by Ca^{2+}	1.72 mg/mL with larchwood xylan	[42]
(*Marinifilaceae* bacterium SPP2)	50	6.0	Purified enzyme	Poor inhibition by 5 mM of $CaCl_2$	0.97 mg/mL with beechwood xylan	[79]
Clostridium thermocellum strain ISO II	65	6.0	Partially purified enzyme	Ca^{2+} improved the enzyme activity at 5.6 mM	2.54 mg/mL with insoluble oat spelt xylan	[80]
C. cellulovorans	45	5.5	Free enzyme	-	7.7-8.3 mg/mL with birchwood xylan	[81]
C. cellulovorans	55	6.5	Whole-cell Immobilized	Ca^{2+} improved the enzyme activity at 5 mM	6.01 mg/mL with beechwood xylan	This work

686

Figure captions

Fig.1**.** Map of pAIDA-xynA plasmid used for the autodisplay of the endo-1,4-β-xylanase using the AIDA system of *E. coli*. Cassette contains of the *gapAP1* promoter (PgapA), the signal peptide CtxB derived from *Vibrio cholera* (SP), followed by the synthetic gene encoding the endo-1,4-β-xylanase (*xynA*) from *C. celluvorans*, and the β-barrel of the autotransporter AIDA (AT-AIDA). Other elements are the origin of replication of pMB1 (Ori) and the β -lactamase gene (bla).

Fig. 2. Colorimetric assay used for detection of the endo-1,4-β-xylanase activity on: (A, B) *E. coli* TOP10/pAIDA-XynA and (C, D) *E. coli* TOP10 cells as negative control. The strains were cultured on a LB agar 24-well plate plus RBB-Xylan for 48 h at 37°C. B and D are the images in gray tones of A and C images, respectively for a better appreciation. The arrows show the hale of substrate hydrolysis.

Fig. 3. a) Determination of optimal pH (6.5) for the endo-1,4-β-xylanase activity. b) Determination of optimal temperature (55°C) for the endo-1,4-β-xylanase activity. Values are expressed as the mean of the percentage of relative activity. Bars represent means ± standard deviations for three replicates.

Fig. 4. Thermal stability of *E. coli*-AIDA-immobilized XynA. Residual endo-1,4-β-xylanase activity was measured after pre-incubation at 60°C (circles), 70°C (squares), and

80°C (triangles), for 15 to 60 min, of cells without (gray lines) and with addition (black lines) of 5mM of $CaCl_2$. Bars represent means ± standard deviations for three replicates.

Fig. 5. Effect of the Ca^{2+} ion on the relative endo-1,4-β-xylanase activity of *E. coli*-AIDA-immobilized XynA. Bars represent means ± standard deviations for three replicates ($p < 0.05$).

Fig 6. Modular structure of XynA from *Clostridium cellulovorans*. (a) Distinct functional domains: glycosyl hydrolase domain from family 11 (GH11), the Dockerin I, and the NodB deacetylase domain. (b) Alignment of conserved feature residue pattern (D [NDT] X X D [DEN] X X D), highlighted in yellow, for calcium binding sites, of the Dockerin I domain from different xylanolytic microorganisms.

Fig. 7. Effect of metallic ions, detergents and organic compounds on *E. coli*-AIDA-immobilized XynA activity. Residual endo-1,4-β-xylanase activity in presence of 1 mM of metals and detergents, 20 mM acetic acid, 10 mM formic acid, or 0.5 mM furfural. Bars represent means ± standard deviations for three replicates.

Fig. 8. Michaelis-Menten type graph showing the initial velocity of the endo-1,4-β-xylanase of *E. coli*-AIDA-immobilized XynA using different xylan concentrations**.** Bars represent means ± standard deviations for three replicates. The small graph shows the liner regression using the reciprocals of substrate concentration ([S]) and the initial velocity (V_o).

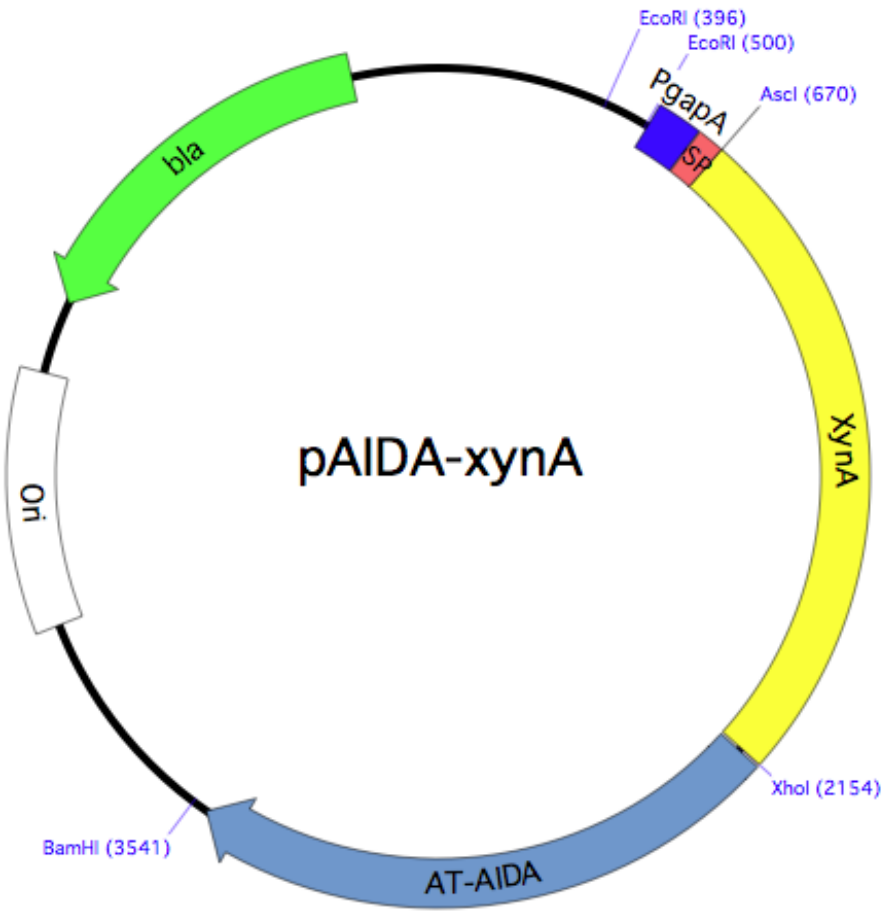
EcoRI (396)
EcoRI (500)
PgapA
AscI (670)
Sp
bla
XynA
pAIDA-xynA
ori
XhoI (2154)
BamHI (3541)
AT-AIDA

Fig. 1

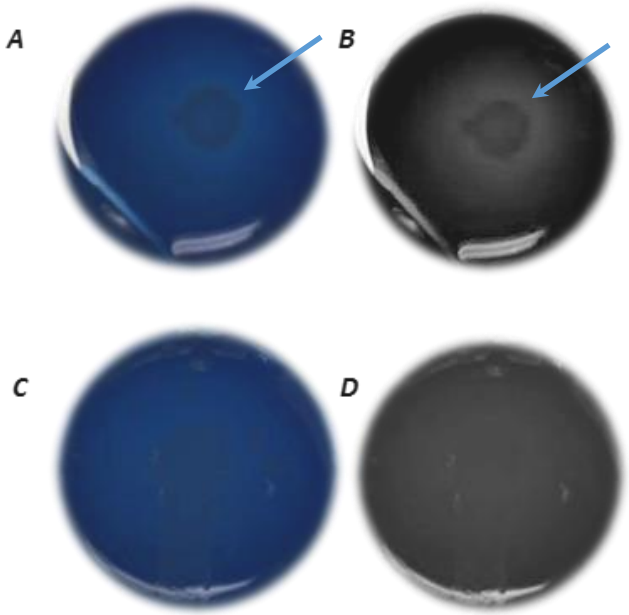

Fig. 2

753

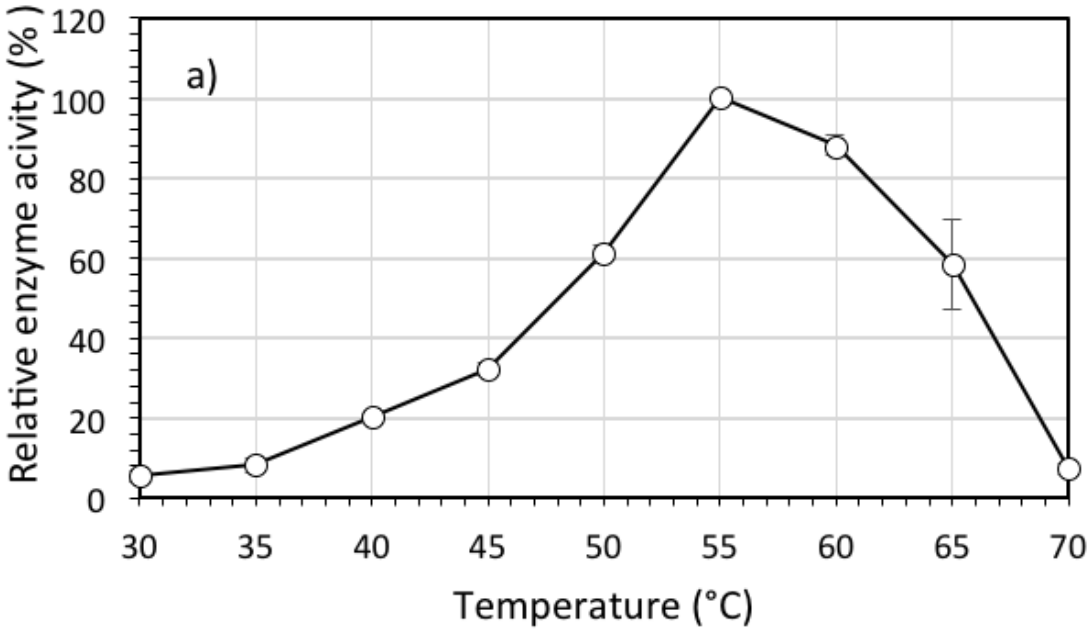

754

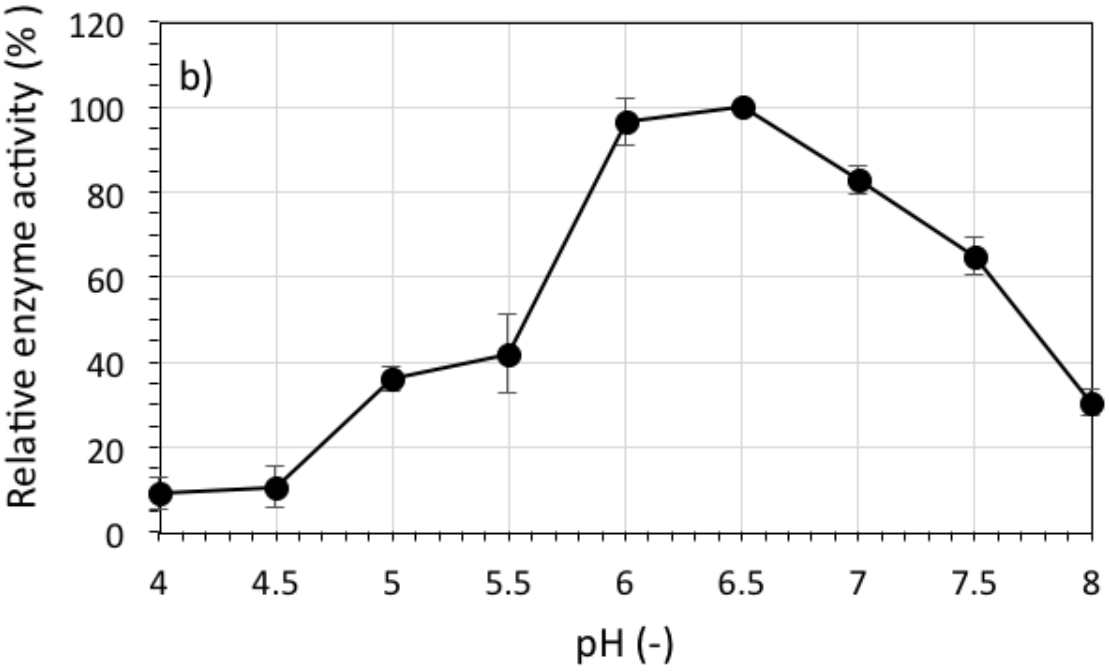

755

756

757 Fig. 3

758

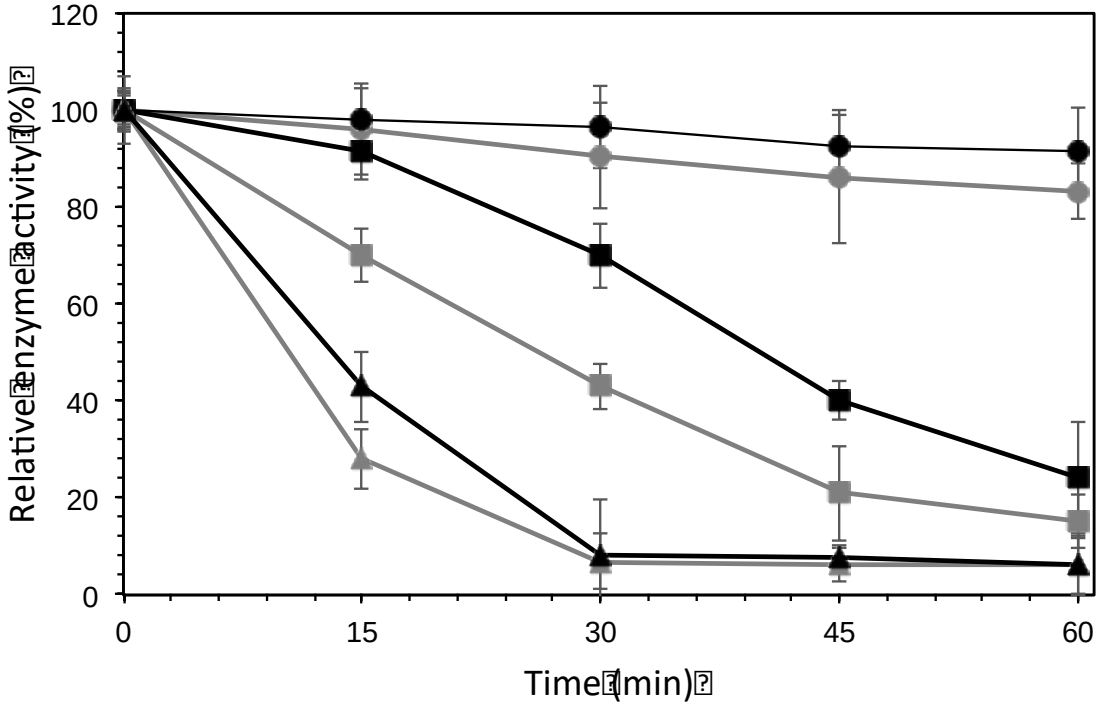
120
100
80
60
40
20
0
Relative enzyme activity (%)
0
15
30
45
60
Time (min)

Fig. 4

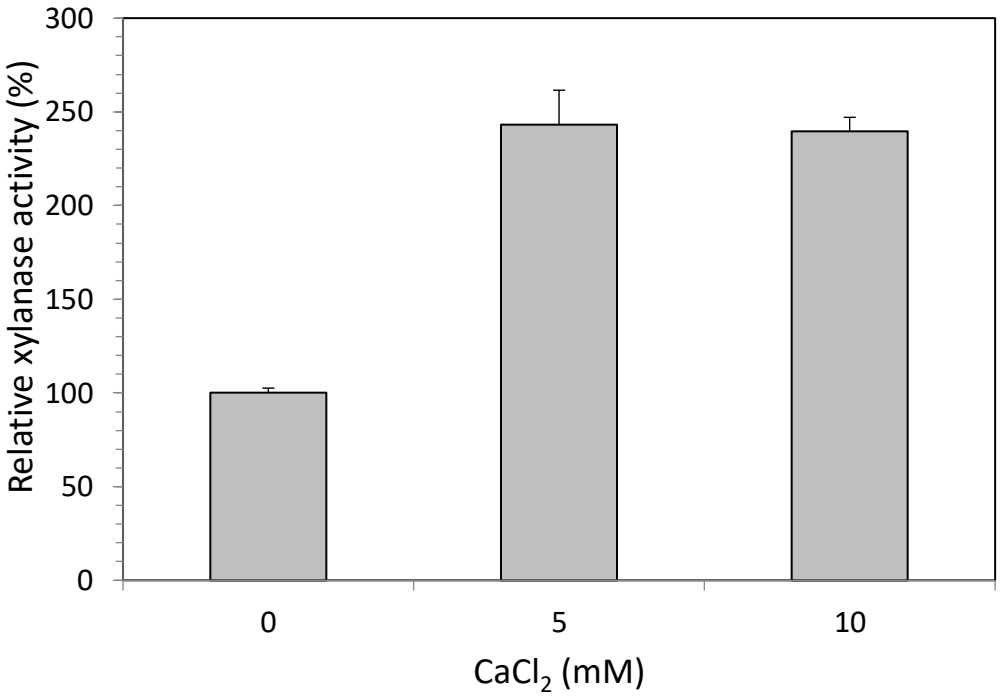
Relative xylanase activity (%)
300
250
200
150
100
50
0
0
5
10
CaCl2 (mM)

Fig. 5

a)

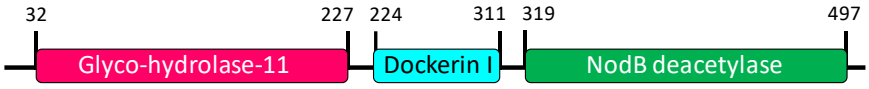

b)

```
   1 YGDVNGDGKVNSADAALLKKYLLG.[ 6].AQLKAADVNGDG.[1].VNAIDLALLKKYLL 57    Dockerin XynA-AIDA Clostridium cellulovorans
   4 YGDYNNDGNVDSTDFAGLKKYIMA.[ 3].AYVKNLDVNLDN.[1].VNAFDLAILKKYLL 57    Clostridium cellulolyticum
   1 MGDVNGDGTINSTDLTMLKRSVLR.[ 6].DAKARADVDKNG.[1].INSTDVLLLSRYLL 57    Clostridium thermocellum
   7 IGDVNADGVVNISDYVLMKRYILR.[ 8].DDMWVGDVNGDN.[1].INDIDCNYLKRYLL 65    Clostridium thermocellum ATCC 27405
 794 YGDVNADGIVDIADTVLLARYIAQ.[ 8].QGLQNADCDPDG.[1].IDSSDLTAIARYLA 852   Ruminococcus sp. 18P13
1985 REDTNADGTVTASDALRVINYMNN.[12].TGWSRLDVNGDG.[1].VTALDALLVINKLN 2047  Rhodopirellula baltica SH 1
 815 LGDINFDGDINSIDYALLKAHLLG.[ 6].DALKAADVDKNG.[1].VNSIDYAKMKQYLL 871   Clostridium clariflavum DSM 19732
 628 YGDANGDGDIDLFDFALIKRALLG.[ 6].IYWKAADCNKDG.[1].LDLFDFAVVKRYIL 684   Eubacterium eligens ATCC 27750
 385 RGDINGDGKLNDTDLEMLRNYLLK.[ 3].KISDKADINMDG.[1].VTMADFVQMNKAIL 438   Ruminococcus albus 7
1973 SGDINGDGKVDIADALLALQMAVG.[14].APLSNGKPAPDG.[1].IDIADAMLILEKAV 2037  Geobacter uraniireducens Rf4
 684 KGDVTGDGTVDIQDYIALQKYILD.[ 4].INAANADVNGDG.[1].VNTADLFALRKMVL 738   Clostridium saccharoperbutylacetonicum ATCC
1985 REDTNADGTVTASDALRVINYMNN.[12].TGWSRLDVNGDG.[1].VTALDALLVINKLN 2047  Rhodopirellula baltica SH 1
 536 RGDVNGDGKISLIDLAMVKSHLLG.[ 6].DSFARADVNGDG.[1].LSLLDLAMIKSHLL 592   Erysipelothrix rhusiopathiae str. Fujisawa
 628 YGDANGDGDIDLFDFALIKRALLG.[ 6].IYWKAADCNKDG.[1].LDLFDFAVVKRYIL 684   Eubacterium eligens ATCC 27750
```

Fig. 6

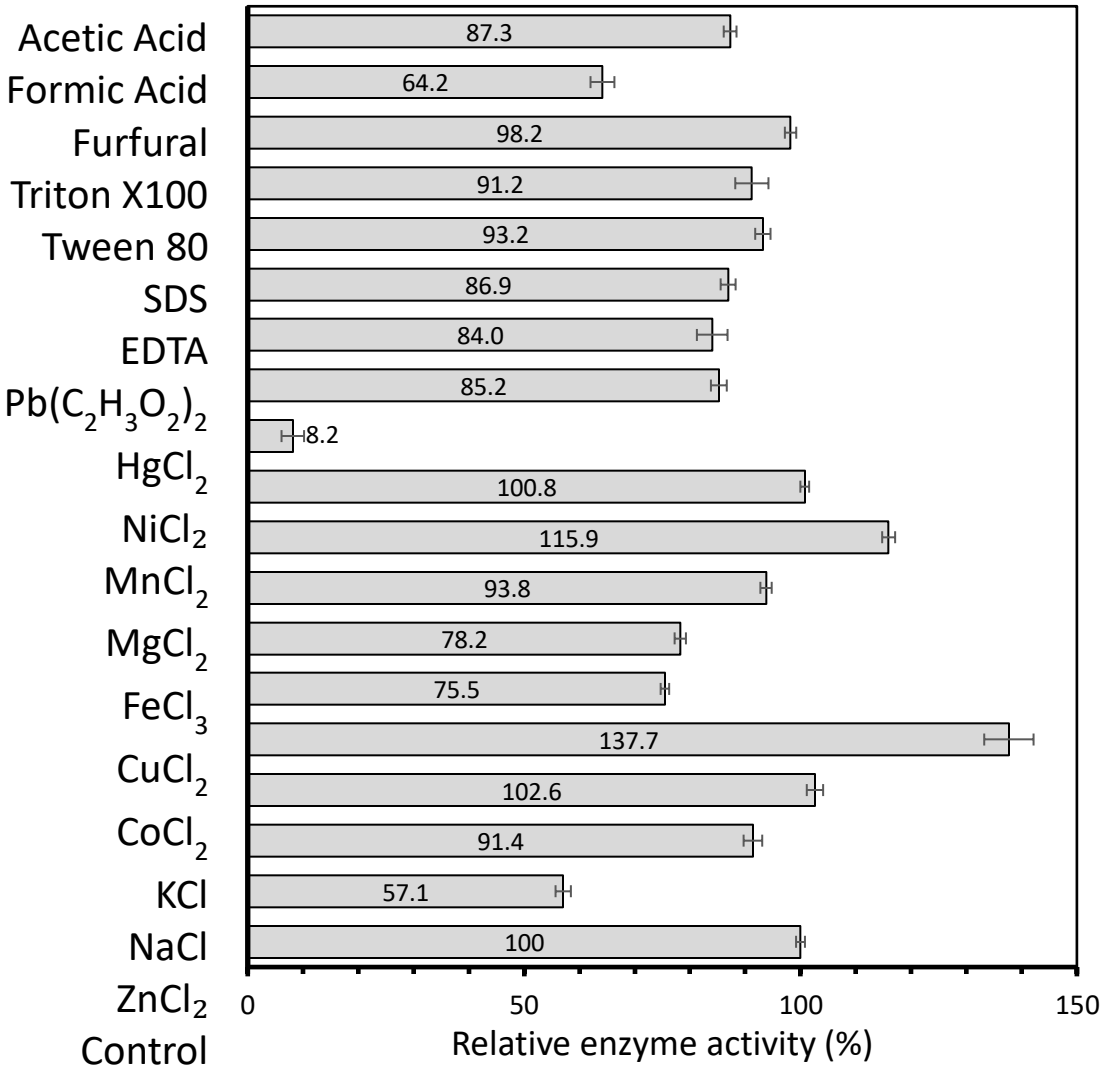
Acetic Acid
Formic Acid
Furfural
Triton X100
Tween 80
SDS
EDTA
Pb(C2H3O2)2
HgCl2
NiCl2
MnCl2
MgCl2
FeCl3
CuCl2
CoCl2
KCl
NaCl
ZnCl2
Control
87.3
64.2
98.2
91.2
93.2
86.9
84.0
85.2
8.2
100.8
115.9
93.8
78.2
75.5
137.7
102.6
91.4
57.1
100
0
50
100
150
Relative enzyme activity (%)

Fig. 7

799

800

801

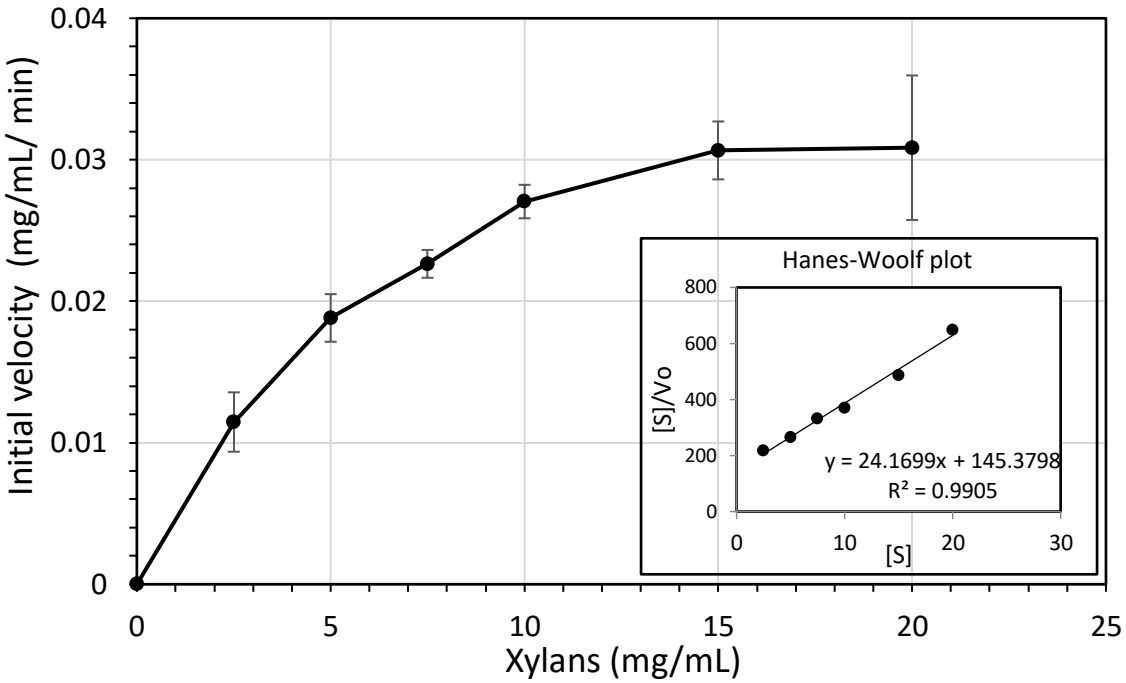

802

803

804 Fig. 8